GEOPHYSICS, VOL. 62, NO. 2 (MARCH-APRIL 1997); P. 540–553, 16 FIGS., 1 TABLE.

Full waveform inversion of marine reflection data in the plane-wave domain

Susan E. Minkoff* and William W. Symes‡

ABSTRACT

Full waveform inversion of a p-τ marine data set from the Gulf of Mexico provides estimates of the long-wavelength P-wave background velocity, anisotropic seismic source, and three high-frequency elastic parameter reflectivities that explain 70% of the total seismic data and 90% of the data in an interval around the gas sand target. The forward simulator is based on a plane-wave viscoelastic model for P-wave propagation and primary reflections in a layered earth. Differential semblance optimization, a variant of output least-squares inversion, successfully estimates the nonlinear P-wave background velocity and linear reflectivities. Once an accurate velocity is estimated, output least-squares inversion reestimates the reflectivities and an anisotropic seismic source simultaneously. The viscoelastic model predicts the amplitude-versus-angle trend in the data more accurately than does an elastic model. Simultaneous inversion for reflectivities and source explains substantially more of the actual data than does inversion for reflectivities with fixed source from an air-gun modeler. The best reflectivity estimates conform to widely accepted lithologic relationships and closely match the filtered well logs.

INTRODUCTION

This paper reports the full-waveform inversion of a small marine data set. The data contain a bright reflecting horizon embedded in essentially flat-lying layers. Little evidence of either multiply reflected energy or mode conversion is observable in the data. On a small scale, energy may be lost to shear motion or other scattering from thin layers, but we treated those effects as a bulk attenuation of the signal. Accordingly, the inversion technique used a plane-wave viscoelastic model for P-wave propagation and primary reflections in a layered earth. A multistage iterative algorithm adjusted model components to minimize the mean-squared misfit between predicted plane-wave data gathers and those extracted by the Radon transform from field midpoint gathers. The algorithm estimated the compressional (or P-wave) background velocity, the anisotropic seismic source, and three elastic reflectivities (or short-scale relative fluctuations in combinations of the P-wave velocity, S-wave velocity, and density). This choice of inversion targets included the background velocity which has a nonlinear effect on the data and thus can have a very large influence on the accuracy of the final answer. It also included parameters that have a linear influence on the data (the elastic reflectivities and seismic source). We did not use inversion to estimate the S-wave background velocity, background density, or attenuation parameters.

To gauge the accuracy of our results, we used several tests. First, well logs provided an independent estimate of two of the three elastic parameters. The background velocity's ability to place the significant events in the reflectivities at the same depth independent of plane-wave slowness (p) provided us with a second, internal measure of consistency. This test is very similar to the use of "coherency" or "common image" panels in migration velocity analysis. Last, we used the relative misfit of the observed to predicted data to compare the inversion results. An initial estimate of the P-wave background velocity obtained by layer stripping in the plane-wave domain proved inferior to the background velocity obtained from waveform inversion. Similarly, an initial estimate of the seismic source obtained from modeling the data collection geometry and air-gun apparatus was less successful in explaining the data than was the inversion result. Finally, we determined that a reasonably accurate quality factor estimate (Q_P) is necessary to achieve an acceptable data fit. In particular, elastic inversion does not explain the dominant amplitude-versus-angle (AVA) trend observed in the data.

The inversion-estimated source we describe here is likely not the physical source one would measure. First, in these experiments we have applied the Radon transform and time

Manuscript received by the Editor May 3, 1995; revised manuscript received December 28, 1995.

*Formerly The Rice Inversion Project, Department of Computational and Applied Mathematics, Rice University, Houston, TX 77251-1892; presently Texas Institute for Computational and Applied Math (TICAM), 2.316 Taylor Hall, University of Texas, Austin, TX 78712.
‡The Rice Inversion Project, Department of Computational and Applied Mathematics, Rice University, Houston, TX 77251-1892.

© 1997 Society of Exploration Geophysicists. All rights reserved.

migration before performing any inversions. A measured source that matched the original data would likely not fit this processed data well. Second, some data attributes were not removed by preprocessing but were also not explicitly included in our model (for example, the influence of the receiver array configuration and ghosts). These features may become part of the source description we obtain from inversion. Nonetheless, when we compare estimates of small-scale features in the elastic parameters based on inversion for velocity model and source to estimates obtained from other velocity analysis and source parameterization techniques, we find that the inversion-based estimates do a substantially better job of conforming to independent measurements (well logs) and to commonly accepted lithological relationships.

The prior work perhaps closest in spirit to our approach is that of Martinez and McMechan (1991a; 1991b) who use a viscoelastic simulator to forward model seismic data as the basis for an inversion algorithm. Part 1 of their paper shows three synthetic examples which contrast elastic and viscoelastic modeling. The modeling technique is layer-based and produces p-τ (plane-wave) seismograms, as does the modeling technique used in this paper.

In part 2 of their paper, Martinez and McMechan apply linearized inversion to estimate the quality factors, shear and compressional wave velocities, layer thicknesses, and densities. They test the inversion on both synthetic and field data. Furthermore, they perform eigenvalue analysis on a simple single-layer model problem that indicates the best and least well-determined of the estimated parameters. In contrast to the work reported here, however, Martinez and McMechan do not determine the energy source as part of their inversion.

The results of Igel (1993) are also related very closely to those described in this paper. In fact, the experiments discussed in this paper used data from the same Gulf of Mexico survey. Igel employed a 2-D elastic finite-difference simulator to invert for the P-wave impedance and Poisson's ratio. He did not invert for either the source or background compressional-wave velocity, relying on other techniques to provide these parameters. By inverting near-offset traces for the P-impedance and then using this result to invert all the traces for Poisson's ratio, he was able to obtain a final misfit error of 44.7%.

Other recent references for full-waveform elastic inversion include Wood (1993) and Pan et al. (1993). Wood estimates the shear velocity, compressional velocity, and density via inversion. Pan et al. include the layer thickness as the fourth parameter sought in the inversion. In all of the above inversion references, however, the source wavelet is either assumed to be known exactly (Wood, 1993) or is estimated from the data via statistical techniques (Martinez and McMechan, 1991a; 1991b, and Pan et al., 1993). Martinez and McMechan mention that inversion could be used to estimate the energy source as well, but they give no examples.

Along with well-known source signature deconvolution techniques such as predictive deconvolution (Robinson, 1967) and homomorphic deconvolution (Ulrych, 1971; Stoffa et al., 1974; Buhl et al., 1974), several authors have discussed estimating the energy source and other parameters via inversion. The references include a talk given by Canadas and Kolb (1986), and papers by Bube et al. (1988), Sacks (1990), and Lewis (1989). Lewis showed that band-limited sources and reflectivities could be estimated by simultaneous inversion. In Minkoff and Symes (1995), we extended Lewis' results to nonconstant background velocities and introduced the numerical technique used in this paper. None of these references, however, combine viscoelastic modeling with energy source estimation.

In short, the work reported here differs from all prior work discussed in the references above on at least one of the following four counts:

1) use of waveform inversion to estimate velocities
2) modeling of attenuation (viscoelasticity)
3) estimation of energy source parameters via inversion
4) simulation of three-dimensional wave propagation.

The next section of this paper explains the viscoelastic, plane-wave, primary-reflection model and the inversion methods based on it which we used in our work. Following the discussion of the forward and inverse methods is a section that provides details about the marine data set used in all the experiments shown in this paper. The remainder of the paper details the experiments we performed starting with the background or long-wavelength velocity inversions and continuing with the source and elastic parameter inversions enumerated in Table 1.

THE METHOD

Modeling

We model the earth as a layered viscoelastic medium and use a convolutional approximation for precritical reflections of viscoelastic plane waves. We do not give the full derivation of the convolutional approximation here. It is related closely to the description of elastic plane waves in Aki and Richards (1980, 153–155); (see also Sacks and Symes, 1987). Christensen (1982) gives a detailed derivation of the viscoelastic equations from physical laws.

The mechanical parameters in the model include the density ρ, the shear and compressional wave velocities v_S and v_P, and the quality factor Q_P. The parameters vary only with depth, $z \equiv x_3$. The time-dependent, anisotropic source is assumed to have, approximately, point support.

Application of the Radon transform (or plane-wave decomposition) to the solution of the viscoelastic wave equation (and to the source and to common-midpoint gathers of the data) reduces the 3-D model to a family of 1-D models (Treitel et al., 1982). In effect, the Radon transform synthesizes incident plane-wave "shot" records parameterized by slowness p and by midpoint. We inverted the reflection angles and frequencies for which the acquisition geometry and equipment produced adequately sampled data for an accurate discretized Radon transform. For typical marine acquisition geometry, Brysk and McCowen (1986) explained how the 3-D transform may be applied to common-midpoint gathers. Following general usage, we shall call this 3-D Radon transformed data p-τ data.

Neither mode conversion nor multiply reflected energy appears to be important in the data (at least on the wavelength scale), most likely because of the soft water bottom in the survey area. This observation suggests that the data might be modeled accurately by a primaries only, or single-scattering, approximation for plane P-waves. This approximation separates mechanical parameters into the long-wavelength (smooth) background velocities and density v_P, v_S, and ρ, and short-wavelength relative perturbations of these parameters, or elastic reflectivities, $r_P = \delta v_P / v_P$, $r_S = \delta v_S / v_S$, and $r_D = \delta\rho/\rho$. High-frequency asymptotics leads to the convolutional model prediction of the P-wave seismogram (Beylkin, 1985); or Sacks and Symes (1987) for elastic plane waves:

$$S^{\text{pred}}(t, p) = f(t, p) * \tilde{r}(t, p). \tag{1}$$

In the above expression, S is the seismogram, f the source wavelet, $\tilde{r}$ the time-slowness domain reflectivity; p denotes slowness, and t time. The "$*$" symbol is convolution in time.

The source wavelet is anisotropic, i.e., slowness-dependent. A convenient representation is a Legendre series in p (which also regulates the extent of its anisotropy):

$$f(t, p) = \sum_{i=0}^{N} f_i(t) L_i(p), \tag{2}$$

where L_i is the ith Legendre polynomial (Abramowitz and Stegun, 1965).

The time-slowness domain reflectivity $\tilde{r}$ is a linear combination of the elastic reflectivities r_P, r_S, and r_D:

$$\tilde{r}(t, p) \approx \int dz [A_P(z, t, p) r_P(z) + A_S(z, t, p) r_S(z) + A_D(z, t, p) r_D(z)]. \tag{3}$$

The geometric optics P-P reflectivity kernels A_P, A_S, A_D are (for $j = P, S$, or D)

$$A_j(z, t, p) = F_j(z, p) \int_{-\infty}^{\infty} d\omega \exp\left[i\omega(t - 2\tau(z, p)) - |\omega| \left(1 - \frac{2i}{\pi} \ln\left|\frac{\omega}{\omega_0}\right|\right) \alpha(z, p)\right], \tag{4}$$

where

$$F_D(z, p) = K_P^2(z, p)[1 - 4p^2 v_S^2(z)], \tag{5}$$

$$F_P(z, p) = \frac{K_P^2(z, p)}{[1 - p^2 v_P^2(z)]}, \tag{6}$$

$$F_S(z, p) = -8K_P^2(z, p) p^2 v_S^2(z), \tag{7}$$

and

$$K_P(z, p) = \frac{(1 - 2v_S^2(z)p^2)\sqrt{(\rho(z)/v_P(z))\sqrt{1 - v_P^2(z)p^2}}}{\rho(z)\left[\left(1 - 2v_S^2(z)p^2\right) + 4v_S^4(z)p^2\left(p^2 + (1/(v_P(z)v_S(z)))\sqrt{1 - v_P^2(z)p^2}\sqrt{1 - v_S^2(z)p^2}\right)\right]}. \tag{8}$$

Table 1. DSO and OLS plane-wave inversion experiments performed on Gulf of Mexico field data.

	Numerical inversion experiment						
Experiment type	DSO		OLS				
Experiment no.	1	2	3	4	5	6	7
Model	viscoelastic		viscoelastic				elastic
Data gather no.	6	6	6	6	6	1,5,7,11	6
Data frequency filtered?	Y	N	Y	Y	Y	Y	Y
Data conditioned?	Y	Y	Y	Y	Y	Y	N
Velocity inversion?	Y		N				
Yes, initial velocity	Fig. 3 dash/dot line						
No, fixed velocity			Fig. 3 dark solid line				
Reflectivity inversion?	Y		Y				
Initial reflectivities	zeros		zeros				
Source inversion?	N	N	N	Y	Y	Y	Y
Yes, initial source				isotropic 15 Hz Ricker			
Yes, final source				isotropic	anisotropic		
No, fixed source	air gun		air gun				
DSO weight	10^{-4}		∞				
Damping weight	10^{-8}		10^{-8}				
Relative residual tolerance	5%		1%				
Alternation rounds	N/A		N/A	2	2	2	2
Relative rms error			55%	53%	29%	30%	33%
Cost function reduction	35%	67%					

The vertical traveltime of plane waves with slowness p is

$$\tau(z,p)=\int_{z_0}^{z} dy \frac{\sqrt{1-[pv_P(y)]^2}}{v_P(y)}. \quad (9)$$

The P-wave attenuation factor at slowness p is

$$\alpha(z,p)=\int_{z_0}^{z} dy \frac{1}{Q_P(y)v_P(y)\{1-[pv_P(y)]^2\}^{1/2}}. \quad (10)$$

The temporal frequency variable is denoted ω; z_0 is the source depth, and Q_P is the P-wave quality factor. The reference frequency ω_0 calibrates the (frequency-dependent) velocity. Waves at frequency ω_0 move with the P-wave velocity v_P. The form of the exponent in the integral expression (4) follows Aki and Richards [1980, p. 182, display (5.88)].

We used the trapezoidal rule to approximate both the complex path integral (4) and the depth-to-time integral (3). The convolution (1) is carried out in the discrete frequency domain by including the Fourier transform of f under the integral in expression (4). The optimization algorithms require the linearization and associated adjoint of the predicted seismogram S^{pred} in v_P as well as the adjoints of the linear operators relating r_P,r_S,r_D, and f to S^{pred}. Application of first-order perturbation theory to the discretized integral transforms (1)–(4) produces the linearization in v_P. Construction of adjoints is straightforward, since all the operators have explicit integral transform representations.

Inversion

The predicted seismogram S^{pred} is linear in each of the parameters f (the seismic source) and r_P, r_S, r_D (the elastic reflectivities). It is very nonlinear in the P-wave velocity v_P. This paper discusses inversion for these five parameters. The predicted seismogram also depends on the (background) S-wave velocity v_S and density ρ, and on the quality factor Q_P, which are treated as fixed and not estimated as part of the inversion. The next section (geometry of the geophysical experiment and preprocessing) describes methods for determining these parameters.

The basic inversion principle embodied in our algorithms is output least-squares (or OLS): This method requires that we adjust the inversion parameters f,r_P,r_S,r_D, and v_P to minimize the mean-squared error

$$J_{\text{OLS}}= \int_{t_{\min}}^{t_{\max}} dt \int_{p_{\min}}^{p_{\max}} dp\, \gamma(t,p)|S^{\text{pred}}(t,p)-S^{\text{obs}}(t,p)|^2, \quad (11)$$

where $S^{\text{obs}}(t,p)$ is the "observed" p-τ data, and $\gamma(t,p)$ is a conditioning weight factor.

The production of the p-τ data set S^{obs} will be discussed in the next section. The conditioning factor $\gamma(t,p)$ enhances the resolution of deeper events. The desired outcome of conditioning permits considerable freedom in the design of the weight. We have used

$$\gamma(t,p)=\exp[|\omega_0|\alpha(z,p)], \quad (12)$$

where $t=\tau(z,p)$ in this formula. Note (from integral expression 10 and expression 12) that in the elastic limit where $Q_P\to\infty$, $\gamma=1$. Thus γ is a model-based gain.

We have used several algorithms to invert for various combinations of parameters. These choices are outlined in the following paragraphs.

Elastic reflectivities.—The influence of the elastic reflectivities (r_P, r_S, and r_D) on S^{pred} is linear, so the mean-squared error is quadratic in these parameters. Since the number of samples is moderately large (approximately 2000 total for the experiments described here), it is natural to use an iterative minimization method. We used the conjugate residual method that monotonically reduces the normal residual (Eisenstat et al., 1983). While the choice of source wavelet influenced the rate of convergence, we were generally able to reduce the normal residual to 1% of its starting value in 20–50 iterations of the conjugate residual algorithm. In all cases, the initial estimates of the reflectivities were zero.

Elastic reflectivities and source parameters.—The source parameters alone have a linear influence on the data, so we applied the same technique to invert for them, namely, conjugate residual iteration. Typically source inversion requires more iterations to satisfy the convergence criterion (reduction of the normal residual) than does elastic reflectivity inversion. This slower convergence appears to reflect the poorer numerical condition of the source inversion problem.

The elastic reflectivities and source parameters *together* have a nonlinear (bilinear) influence, so quadratic minimization algorithms cannot be used directly. Instead, we used a method known as coordinate search or alternation. This method of simultaneous inversion for source and reflectivities was introduced in the paper by Minkoff and Symes (1995). We will hereafter refer to a "round of alternation" to be one pass through the four steps of the following algorithm.

Repeat until convergence:

1) Given the current source f_c and current reflectivity r_c, invert for a new estimate of the reflectivity r_+.
2) Replace r_c by r_+.
3) Given the current source and reflectivity guesses f_c, r_+, invert for a new estimate of the source f_+.
4) Replace f_c by f_+.

In the above algorithm, $r=(r_P,r_S,r_D)$ is the vector of elastic reflectivities. Alternation, although notoriously inefficient, is attractive for initial experiments because it requires only successive solution of simple linear least-squares problems. Quasi-Newton methods could be applied to the problem and would likely reduce the number of iterations dramatically. While further algorithmic development for source-reflectivity inversion definitely is needed, we were able to obtain usable results in many cases with two to three rounds of alternation.

Minkoff and Symes (1995) showed that inversion for an isotropic source and acoustic reflectivity gives unique and even stable results, provided that the slowness range is sufficiently large and the scales of the (background) velocity and reflectivity are sufficiently well separated. Evidently, the introduction of source anisotropy and elastic reflectivity will result in less constrained inversion estimates. Several factors in our approach tend to impose additional constraints on the solution, however. These constraints include the number of terms used in the Legendre series (2) for $f(t,p)$ (which limits the degree of anisotropy), the length of the source time series (which was shorter than the length of the seismic traces), and the truncation of the iterative least-squares conjugate direction solver after a relatively small number of steps which has a well-known regularizing effect. Pending a mathematical study of this issue, experiments like those reported below must be regarded as exploratory.

Elastic reflectivities and P-wave velocity.—The P-wave velocity has a strongly nonlinear influence on the data. Therefore the output least-squares objective function J_{OLS} tends to be very complex. Gradient-based optimization algorithms typically have difficulty converging to useful estimates of velocity and reflectivity (Gauthier et al., 1986; Symes and Carazzone, 1992).

A modification of the OLS approach appears to make it much more amenable to gradient-based optimization. The essential changes are these:

1) *Split* the optimization into *stages*: i.e., for each velocity estimate, invert first for the elastic reflectivities in an *inner optimization*. Then treat the remaining error (*reduced objective*) as a function of velocity, and optimize over velocity.
2) *Relax* the model by permitting the reflectivity components r_P, r_S, and r_D to depend on the slowness ("shot" parameter) as well. This modified inversion will produce a reflectivity "volume" quite analogous to the image volume of prestack depth migration.
3) *Penalize* the variation of reflectivity components with slowness by adding a *differential semblance* term to J_{OLS}:

$$J_{\mathrm{DSO}} := J_{\mathrm{OLS}} + \sigma^2 \iint dp\, dt \times \left\{ \left|\frac{\partial r_P}{\partial p}\right|^2 + \left|\frac{\partial r_S}{\partial p}\right|^2 + \left|\frac{\partial r_D}{\partial p}\right|^2 \right\}. \qquad (13)$$

The *semblance weight* σ^2 regulates the emphasis on semblance. As $\sigma \to \infty$, the objective functions J_{DSO} and J_{OLS} become equivalent:

$$\min_{(r_P, r_S, r_D)} J_{\mathrm{OLS}} = \lim_{\sigma\to\infty} \min_{(r_P, r_S, r_D)} J_{\mathrm{DSO}}. \qquad (14)$$

On the other hand, the opposite limit $\sigma \to 0$ completely decouples the reflectivity inversions for various slownesses. In effect, minimization of J_{DSO} for $\sigma \sim 0$ ("low DSO weight" below) produces independent inversions for each p. This amplitude-corrected image volume is a useful diagnostic tool for velocity quality control, like its analog in conventional migration velocity analysis.

The choice of the semblance weight σ^2 regulates the shape of the objective function J_{DSO}. This weight is best viewed as a Lagrange multiplier for a certain constrained formulation of inversion velocity analysis. In the experiments reported here we set σ by trial and error.

The reduction of the OLS objective function [step (1) above] already appears to eliminate most of the irregular behavior reported in the literature on output least-squares inversion, and suggests that the use of very costly stochastic optimization methods, as has been advocated by a number of authors (for example Scales et al., 1991; Sen and Stoffa, 1991b; 1991a) can safely be avoided. The relaxation and differential semblance steps (2) and (3) tend to enhance considerably the convexity of the objective. For discussion and examples, see Symes and Carazzone (1991), Song (1994), and Gockenbach et al. (1995), and references cited therein. The algorithm just described has been given the name *differential semblance optimization* or DSO. This algorithm consists of two stages: (1) an *inner optimization* for elastic reflectivities r_P, r_S, r_D, which for the examples in this paper was performed via conjugate residual iteration; (2) an *outer optimization* over P-wave velocity v_P of a reduced objective produced by the inner optimization. We have used a version of (nonlinear) conjugate gradient optimization described in Fletcher (1980) to perform the outer optimization. See Kern and Symes (1994) for a discussion of the algorithmic details of DSO.

SEISMIC FIELD DATA—GEOMETRY OF THE GEOPHYSICAL EXPERIMENT AND PREPROCESSING

In this work, we used data derived from a marine survey of the Gulf of Mexico. The survey line consisted of 511 shots recorded with 301 hydrophone groups. The group interval was 15 m with a minimum source-receiver separation of 148 m. The shot interval was 22.5 m. Each group contained 17 equally spaced and equally weighted hydrophones. The data were recorded without a low-cut filter. A 110 Hz high-cut filter was applied. The sampling rate was 2 ms, and the total record length was 5 s.

The data show a strong gas-sand-related direct hydrocarbon indicator readily visible in the stack at about 2.3 s (see Figure 1). The stack shows this target horizon to be embedded in a sequence of nearly horizontal strata, beginning at roughly 1.5 s. Therefore, layered medium modeling appeared to be a plausible tool for target-oriented inversion. Very little evidence of multiply reflected energy appears above or near the target event, suggesting the viability of a primaries-only approach. Similarly, the apparent absence of mode-converted events justifies restriction of the propagation model to P-waves. These hypotheses seem justified a posteriori by the success of the inversions.

The data were Radon transformed, respecting 3-D cylindrical symmetry, to yield 48 plane-wave traces per midpoint gather. Slowness values range from $p_{\min} = 0.116$ ms/m to $p_{\max} = 0.365$ ms/m. To remove diffraction artifacts originating in the shallow subsurface, the plane-wave data were time migrated in the midpoint dip domain. We intended this step to collapse diffractions while still preserving layered reflection amplitudes. The stack shown in Figure 1 is constructed from these migrated and remodeled p-τ data. While the diffracting structures are still clearly visible in the upper 1.5 s, the diffraction tails are largely removed and no longer interfere with the lower, layered structure in the stack. The same is largely true of the prestack p-τ data (see Figure 2).

Techniques other than inversion supplied alternate estimates of several parameters. A layer-stripping method produced a piecewise constant velocity by flattening p-τ migrated events in selected windows. This approach to velocity analysis is the p-τ analog of a common method for estimation of interval velocities using prestack migration. The result of this layer-stripping velocity analysis is shown as the dashed line in Figure 3.

Also, air-gun modeling software gave an a priori estimate of the source signature and radiation pattern. Figure 4 shows this air-gun model source over the range of slowness values used in the data with every fourth trace displayed for clarity.

To lighten the computational burden of inversion, we performed most of our calculations on a low-pass filtered version of the p-τ data that resulted from convolving all the traces with a 15 Hz zero-phase Ricker wavelet. A single midpoint gather of the filtered data is shown in Figure 2. We also filtered the corresponding air-gun model source. Consequently, this filtered source no longer has the causality and minimum phase properties usually expected of air-gun sources. (The unfiltered source does possess these attributes.)

All of the numerical experiments described in this paper were performed on one or more of eleven selected midpoint gathers. The midpoints were spaced 37.5 m apart, so the total distance from the first to the last midpoint in this subset was 375 m. We label these midpoint gathers CMP1–CMP11. A logged well is near CMP6, and most of our results concern this single midpoint gather.

For the well near CMP6, we obtained block sonic and density logs in the 1.4–2.6 s (two-way time) interval. We have used these logs in assessing the accuracy of the inversions (see Figures 6, 9, 12).

The quality factor was estimated by roughly matching the rate of energy decay in the data with predictions from log-derived synthetics. In the viscoelastic experiments described in this paper, we used a constant value of 90 for Q_P. We have also assumed that v_S and ρ are known with sufficient accuracy from logs and regional relationships which hold on the average over long scales. While these assumptions appear to have permitted accurate inversions, we did not test these assumptions extensively. In particular, we did not attempt to invert for Q_P.

We represented the source by a 31-term Legendre series, settling on this number of terms after a preliminary series of experiments that indicated that many fewer than 30 terms would not permit inversion to fit the amplitude-versus-angle behavior of the data. The source was centered at 0 ms and covered a total time of 500 ms, which was the same as the time window used by the air-gun modeling package.

NUMERICAL EXPERIMENTS—VISCOELASTIC INVERSION IN THE PLANE-WAVE DOMAIN

Discussion of results

1) *The inversion-estimated P-wave background velocity places the significant events in the inverted reflectivities at the same depth location across different slowness values.*

In experiment 1, we used DSO inversion with a semblance weight of 10^{-4} to estimate the P-wave background velocity shown in Figure 3 (dark solid line) from the filtered data shown in Figure 2. The reflectivities, also estimated in this experiment, are allowed to depend on slowness p (as described in the subsection on inversion). To evaluate the correctness of the inverted velocity, we reinverted for the reflectivities only (OLS inversion), this time with very low DSO weight (10^{-9}), which produced a z-p coherency or common image panel (Figure 5). The main feature in the P-wave impedance panel (Figure 5a)

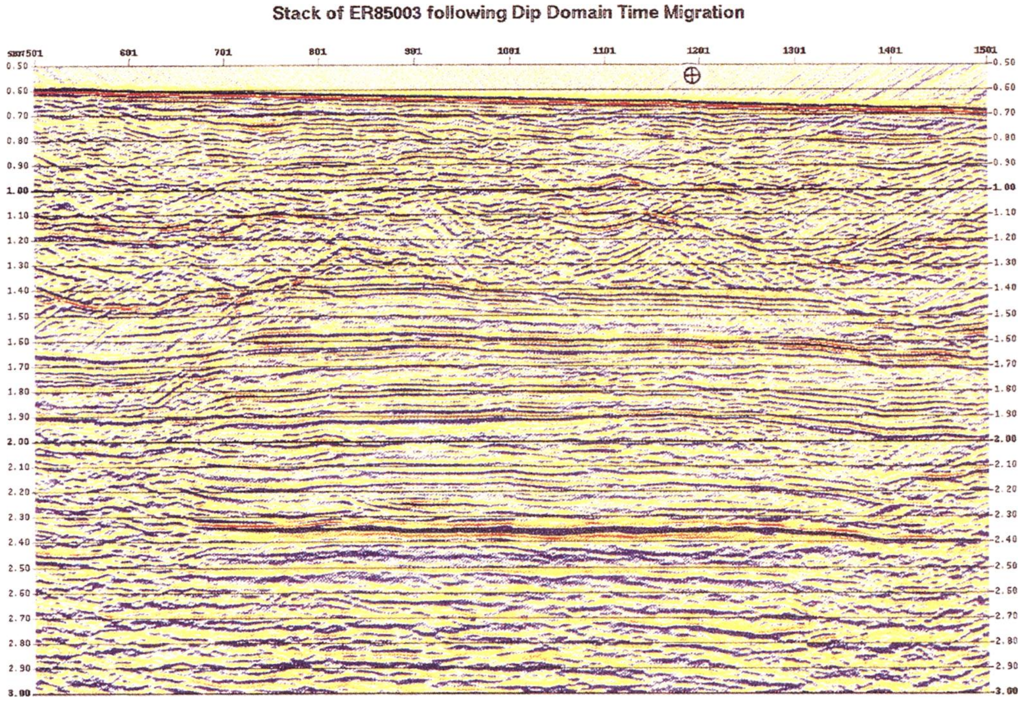

FIG. 1. The stacked section of marine data. The diffracted energy originating in the shallow subsurface was suppressed by prestack time migration in the offset-midpoint slowness domain. Modeling recreated the data with zero midpoint slowness. The location of the logged well referenced in the text is marked. Note that the bright reflecting horizon, a gas sand between 2.3–2.4 s, is embedded in a flat-lying sequence.

is located between 2100 m and 2200 m and appears quite flat. For comparison, we show in Figure 3 (dashed line) the background velocity derived via layer stripping in the p-τ domain. Figure 5b is the P-wave impedance from an inversion with this background velocity and DSO weight 10^{-9}. It also appears quite flat.

2) *The depth of the most significant event in the inverted reflectivity is close to the depth of this event on the sonic well log.*

The gas-sand feature is located at about 2100 m on the logs. The inverted background velocity places this event closer to 2150 m (Figure 4a); whereas the background velocity generated by layer stripping moves it towards 2200 m (Figure 4b).

3) *DSO inversion performed on full bandwidth data still produces a background velocity which flattens significant events across p-dependent traces.*

Using unfiltered CMP6 data, we ran a DSO inversion test for the P-wave background velocity and reflectivities (experiment 2). Although we were not completely satisfied that we had pushed this inversion to its stopping point, the resulting velocity estimate can be seen in Figure 3 (solid line) and is very close to the velocity derived from inverting the filtered data (dark solid line). Moreover, this background velocity estimate rendered the significant events in the coherency panel (low DSO weight inversion for reflectivity) relatively flat across traces.

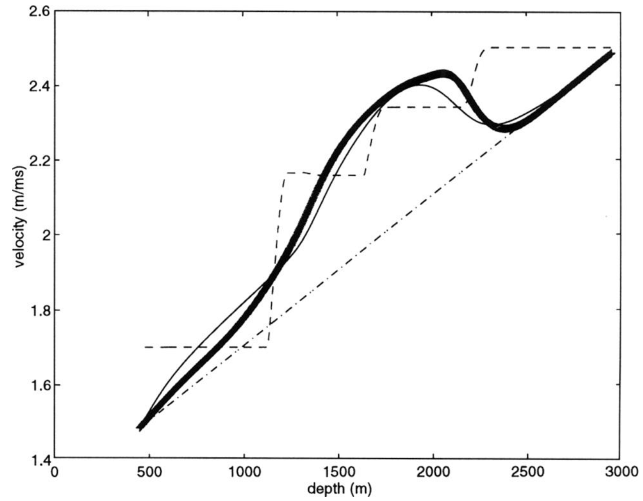

FIG. 3. Dashed/dotted line: Initial estimate of P-wave background velocity used for inversion of common-midpoint data gather 6 (experiments 1 and 2). Dashed line: Background velocity predicted for the same data set using layer stripping in the p-τ domain. Solid line: P-wave background velocity determined via inversion for *unfiltered* CMP6 (experiment 2). Dark solid line: Background velocity estimated from performing the same inversion on *filtered* CMP6 data (experiment 1).

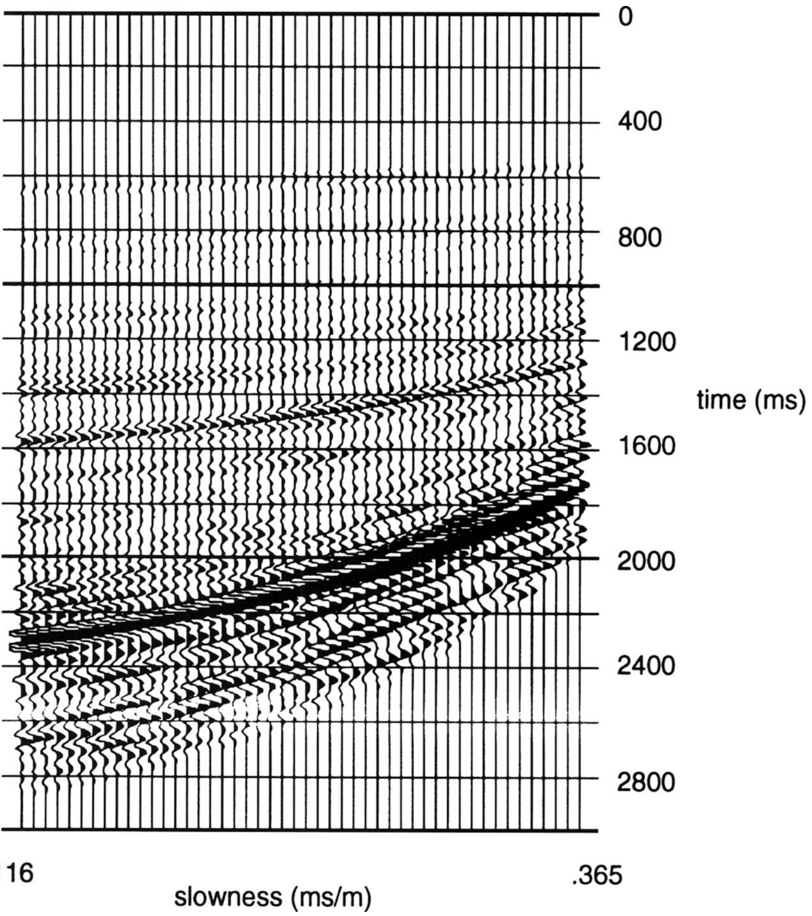

FIG. 2. The τ-p transformed seismic data from common midpoint gather 6. We filtered the data by convolving it with a 15 Hz Ricker filter.

4) *Although we initially assumed the air-gun model source estimate (see Figure 4) to be a good guess for the wavelet, we found that we were able to greatly improve the fit to data by deriving a new source via inversion.*

Holding the P-wave background velocity fixed, we performed three OLS inversions for the elastic reflectivities. In experiment 3, we did not reestimate the energy source in the process of inverting the reflectivities. The normalized misfit between actual and predicted data is 55% and the data residual is shown in Figure 7. The residual graphs were all plotted on the same scale as the observed data. It is clear from the graph of the misfit that the reflectivities estimated using the air-gun model source do not accurately predict the target event for large slowness values.

Experiments 4 and 5 are identical to experiment 3, except that we estimated both the three elastic parameter reflectivities *and the energy source* using inversion. In experiment 4, we constrained the energy source to be isotropic. The initial guess for the isotropic wavelet is shown in Figure 8a, and the final source wavelet estimated in this experiment is shown in Figure 8b. In two rounds of the alternation algorithm applied to CMP6, the normalized misfit error was reduced to 53%. The residual graph makes manifest the fact that an isotropic source (even one determined by inversion of a fully elastic reflectivity model) does not permit a good fit to data at the gas-sand event (see Figure 10).

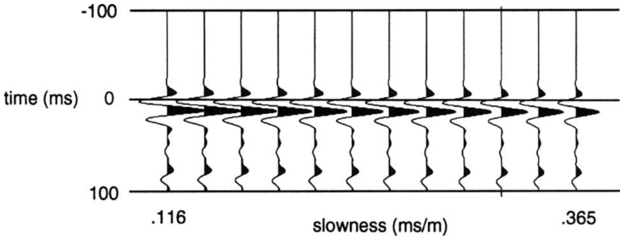

FIG. 4. The air-gun model source estimate with every fourth trace shown.

Finally, in experiment 5 we estimated the reflectivities and an *anisotropic* (or p-dependent) energy source via inversion. In two rounds of alternation, we reduced the normalized misfit error to 29%. (In fact, in a 200 ms window around the gas-sand event, this inversion matched all but 11% of the data.) The source estimate is shown in Figure 11, the residual in Figure 13.

Similarly, we inverted the individual data gathers CMP1, CMP5, CMP7, and CMP11 in four separate experiments and achieved data fit errors of at most 30% after only two rounds of alternation (see the experiments described in Table 1 under "experiment 6"). Thus we see that we can explain 25% more of the seismogram by allowing the earth parameters *and the source* to be estimated from the data.

5) *Of the three sets of estimated reflectivities (experiments 3–5), the reflectivities from experiment 5 that were generated by the inversion-estimated anisotropic energy source most closely match the well logs.*

The linearized inversion method assumes that a separation of frequency content exists between the background (low-frequency) density and velocities and the (high-frequency) reflectivities. To gauge the accuracy of our reflectivity estimates, we therefore found it necessary to detrend the well logs. We subtracted a smooth average of the log from the original and then turned the logs into (dimensionless) reflectivities by dividing this difference by the smooth average. Figure 6 compares the detrended sonic velocity log (dashed line) to the short-scale relative fluctuation in the P-wave impedance calculated from inversion (solid line) for experiment 3. The reflectivity-log

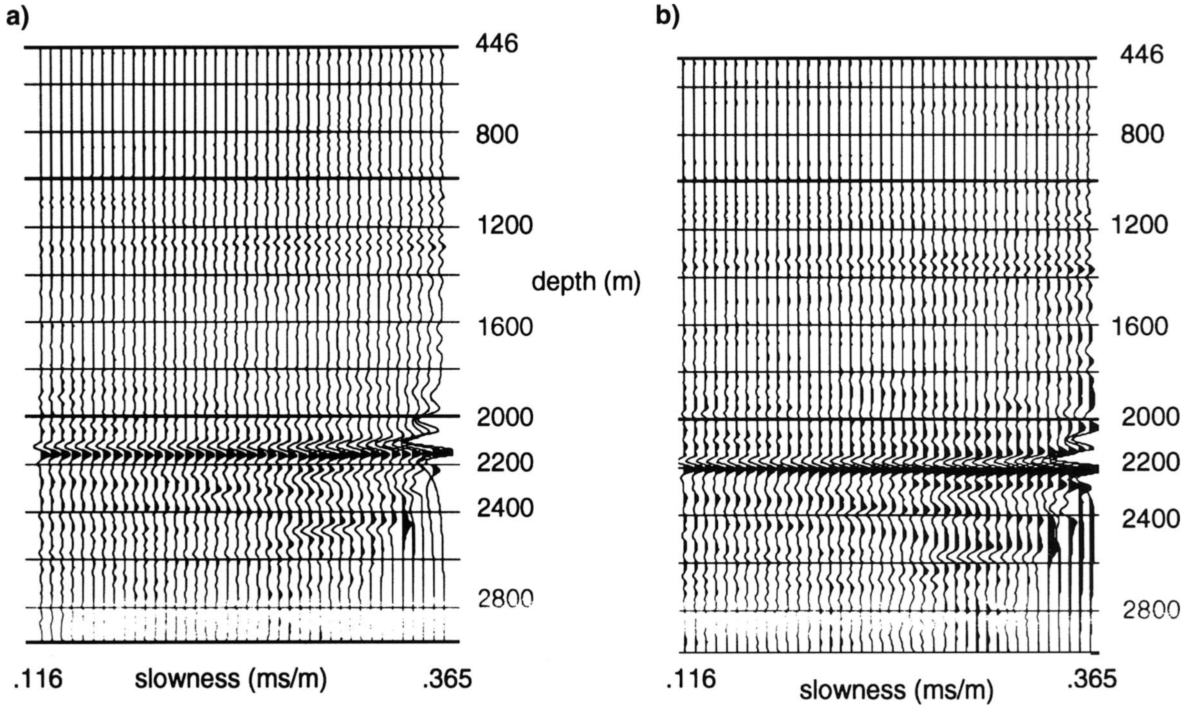

FIG. 5. (a) The P-wave impedance resulting from a "low DSO weight" inversion, the fixed (air-gun model) source, and the inversion-estimated background velocity shown in Figure 3 (dark solid line). (b) The P-wave impedance that results from using the layer-stripping background velocity shown in Figure 3 (dashed line).

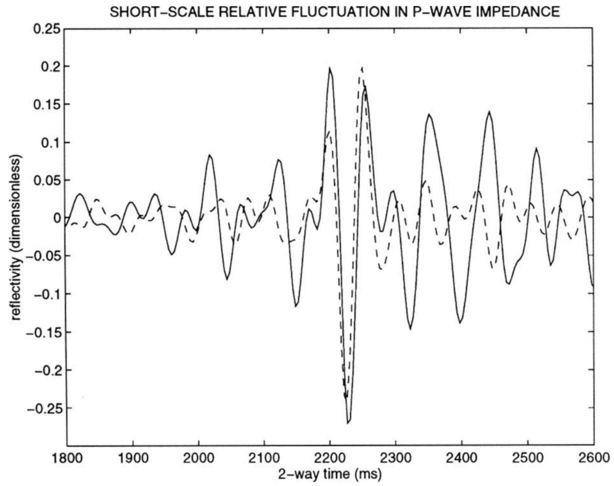

FIG. 6. Comparison of the independent well-log measurement of the relative short-scale fluctuation in the P-wave impedance with the result of inversion done on CMP6 using the air-gun model source estimate (experiment 3). The solid line shows the inversion result (scaled and shifted left 20 ms). The dashed line shows the detrended well log. Both graphs have been plotted as a function of two-way time and filtered to match the frequency content of the source.

comparisons are all plotted as a function of two-way time and filtered using a zero-phase 8–32 Hz tapered Ormsby frequency filter (corresponding roughly to the passband of the source). For this experiment, we shifted the inverted reflectivities 20 ms towards $t = 0$ and scaled the peak amplitudes so that the log and inversion results could be overlaid and their shapes compared.

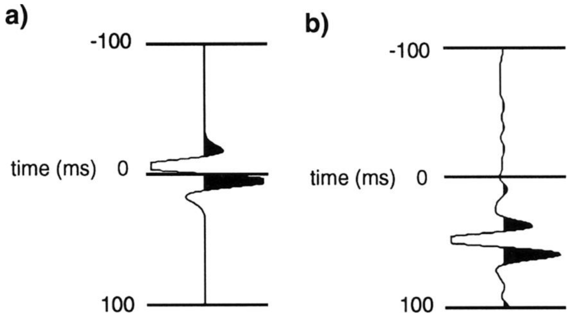

FIG. 8. (a) The initial source guess (derivative of an isotropic Ricker wavelet) used in inversion experiments 4 and 5. (b) The isotropic inversion-estimated source resulting from experiment 4.

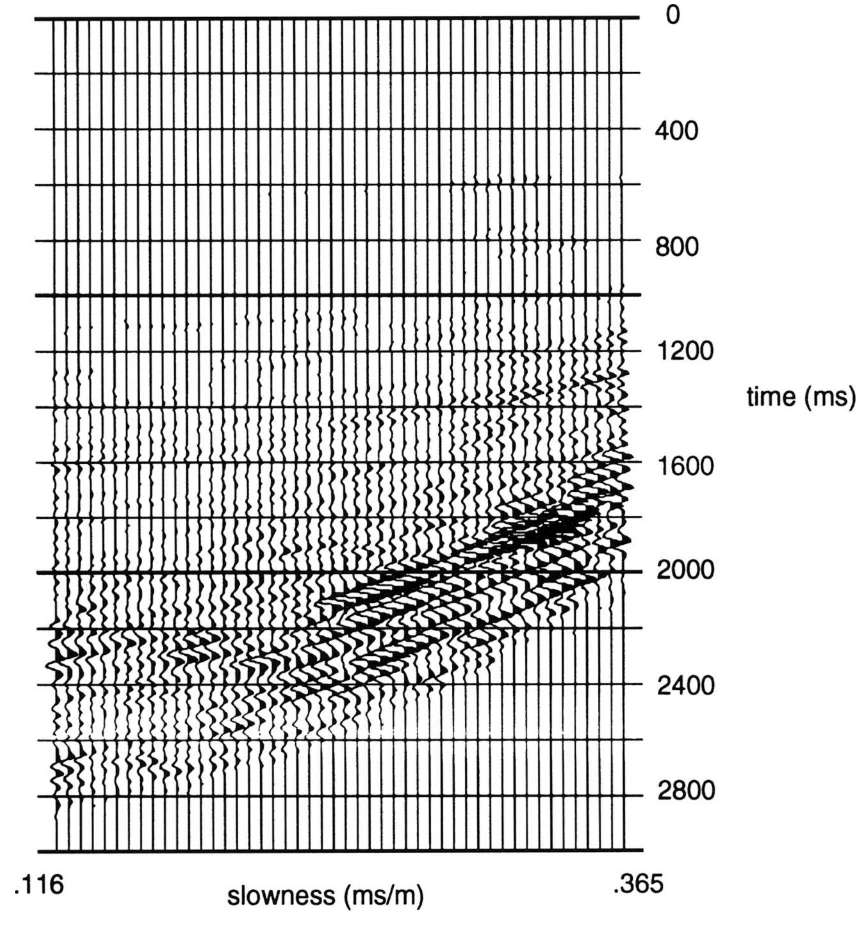

FIG. 7. Difference between the actual data (CMP6) and the data predicted by inversion-estimated reflectivities using the air-gun source (fixed background velocity) (experiment 3). The misfit in the prediction is 55% and is plotted on the same scale as the CMP6 data.

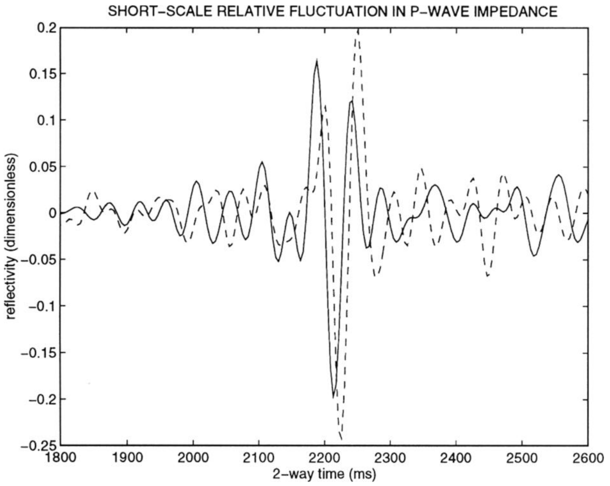

FIG. 9. Comparison of the independent well-log measurement of the relative short-scale fluctuation in the P-wave impedance with the result of inversion done on CMP6 using an isotropic source estimate from inversion (experiment 4). The solid line shows the inversion result (scaled and shifted left 67 ms). The dashed line shows the detrended well log. Both graphs have been plotted as a function of two-way time and filtered to match the frequency content of the source.

Figure 9 shows the comparison between the well log and inversion result for P-wave impedance from experiment 4. We shifted the inverted reflectivity 67 ms toward $t = 0$. The larger time shift was needed here most likely because our inversion algorithm (alternation) was not powerful enough to change the initial (slightly erroneous) time origin of the source by this amount.

Finally, the parameter estimate versus log for experiment 5 is shown in Figure 12. Again, this inversion result was scaled and shifted 67 ms toward $t = 0$ to facilitate comparison to the log measurements. Clearly, these comparisons improve with the addition of an inversion-estimated source and especially when this source is allowed to be anisotropic.

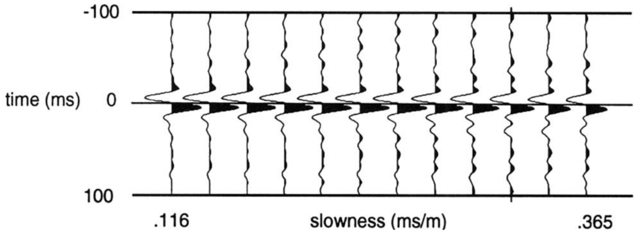

FIG. 11. The estimated anisotropic source from the linear source-reflectivity inversions where only every fourth trace is shown for clarity (experiment 5).

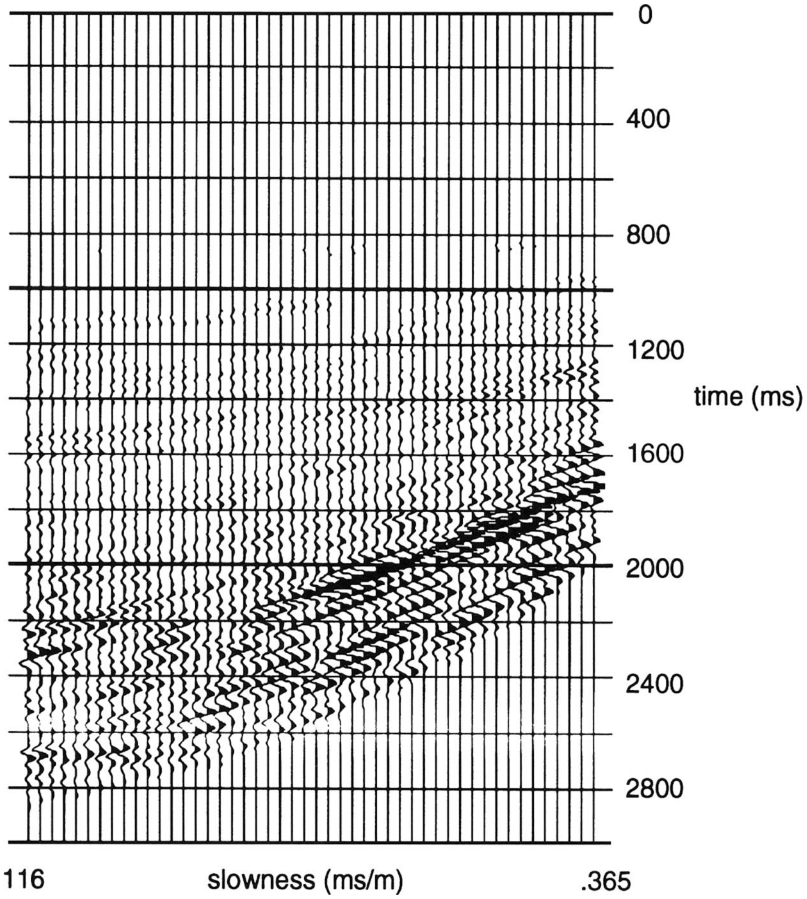

FIG. 10. Difference between the actual data (CMP6) and the data predicted by inversion using an isotropic inversion-estimated source (fixed background velocity) (experiment 4). The misfit in the prediction is 53% and is plotted on the same scale as the CMP6 data.

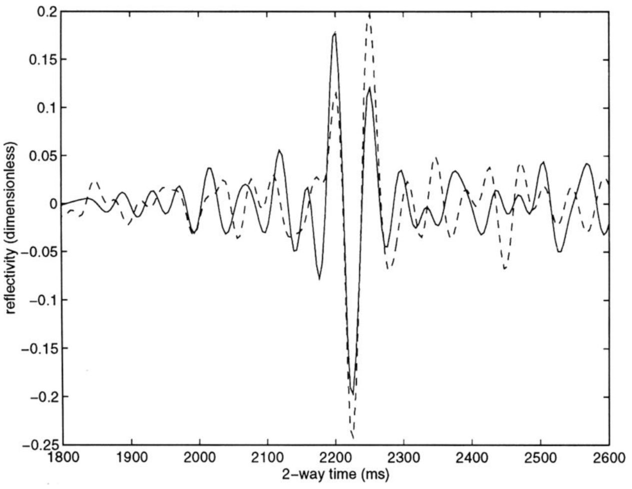

FIG. 12. Comparison of the independent well-log measurement of the relative short-scale fluctuation in the P-wave impedance with the result of inversion done on CMP6 using an anisotropic source estimate from inversion (experiment 5). The solid line shows the inversion result (scaled and shifted left 67 ms). The dashed line shows the detrended well log. Both graphs have been plotted as a function of two-way time and filtered to match the frequency content of the source.

Shear velocity logs were not available for us to use for comparisons. Although agreement of the inversion-estimated parameters with the *measured* logs is generally good, none of the experiments described do an adequate job of matching in detail the shear log calculated from Castagna's relation. This relation does not hold for gas sands (our target event); see Castagna et al. (1985). In fact the shear modulus in this target range of 2200–2300 ms should be nearly constant. Figure 15 shows that the inverted shear moduli from experiments 4 and 5 (inverted source) do a better job of conforming to this expectation than does the modulus resulting from experiment 3 (air-gun modeled source).

6) *Inversion results for the anisotropic inversion-estimated source and reflectivities show that the* v_P/v_S *reflectivity is relatively constant and near zero except at the gas sand where it is more negative than the* v_P *reflectivity.*

Castagna and Smith (1994) postulate that this v_P/v_S indicator is more dependable than traditional AVO gas-sand indicators such as the P-wave velocity. Their hypothesis comes from examining velocity and density well log data from 25 sets of samples. The measurements were of adjacent shales, brine sands, and gas sands. Our inversion results agree with their conclusion. See Figure 14 that compares six elastic reflectivities from experiment 5.

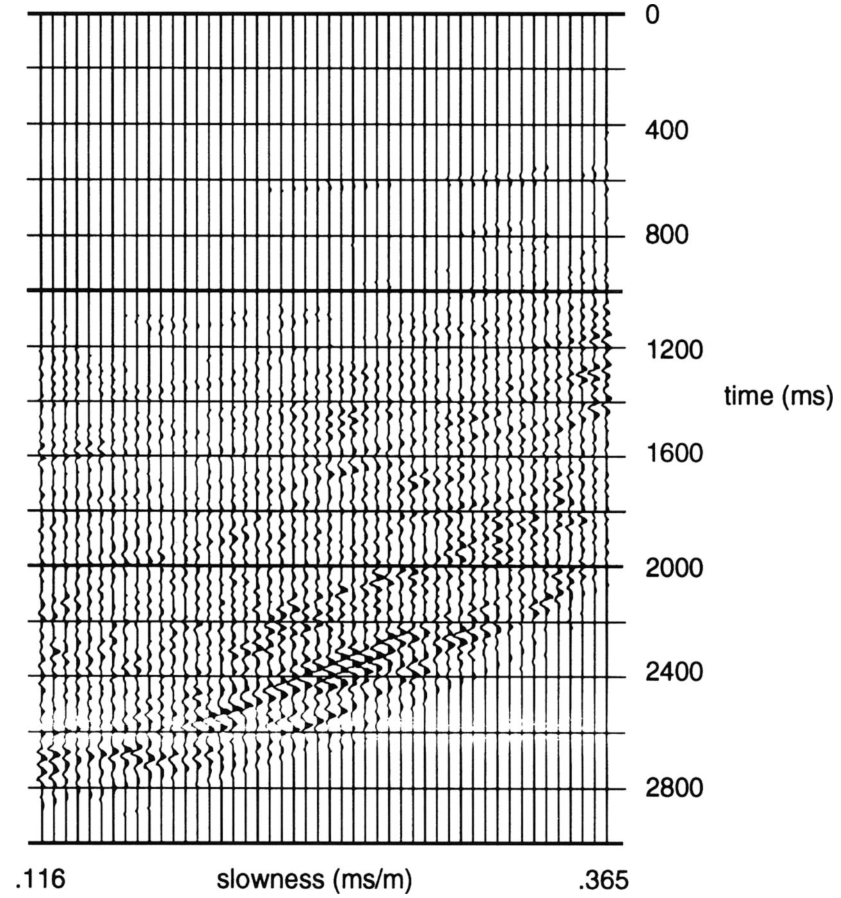

FIG. 13. Difference between the actual data (CMP6) and the data predicted by inversion using an anisotropic inversion-estimated source (fixed background velocity) (experiment 5). The misfit in the prediction is 29% and is plotted on the same scale as the CMP6 data.

7) *The viscoelastic model allows a better fit to this seismic data set than does an elastic modeler.*

To test the importance of modeling attenuation for this data set, we inverted for a fully anisotropic energy source and the same three reflectivities using ungained data and a very large quality factor ($Q_P = 10000$). (In all other experiments, we used the smaller value of $Q_P = 90$.) The background velocity was the velocity in Figure 3 (dark solid line). Inversion for source and elastic reflectivities after two rounds of alternation reduced the root-mean-squared error to 33% of the data norm. However, one notes from the residual (Figure 16) that the parameters estimated via elastic inversion do not predict the amplitude-versus-slowness trend in the data. For large slowness values, the target event can still be seen clearly in the residual. In fact, most of the misfit (25% of the data norm) lies in the target interval (2200–2400 ms).

CONCLUSION

In this paper, we have shown that we were able to estimate parameters in a model of marine τ-p transformed seismic data in both linear and nonlinear ways by a completely deterministic approach. In a sequence of steps, we inverted for the P-wave background velocity, the seismic energy source, and three elastic parameter reflectivities. The viscoelastic modeler used assumed a layered medium and single scattering. The results were conclusively in favor of using the data directly (via inversion) to estimate as much as possible about the model. We were able to predict the most significant event in the P-wave impedance log accurately. The background velocity estimate placed the events in the reflectivity panels at the same depth location across traces. By inverting for the energy source as well, we were able to fit 70% of the seismic data. In fact, in a small window around the target, we were able to fit 90% of the seismic data in a single CMP data gather. The attenuative model gave a much better account of amplitude-versus-angle dependence in the data than did linear elasticity—an elastic inversion fit only 75% of the data in the target zone. With viscoelastic modeling and an inversion-estimated anisotropic source, we obtained parameter relations closely conforming to those predicted from lithology.

ACKNOWLEDGMENTS

The authors thank Exxon Production Research Co. for making the data used in this study available to us. We are indebted to James J. Carazzone of EPR Co. for his invaluable advice and assistance. We also express our appreciation to Robert Baumel, William Harlan, Ruben Martinez, Warren Wood, and an anonymous reviewer for many helpful comments and suggestions. This work was partially supported by the National Science Foundation, the Office of Naval Research, the

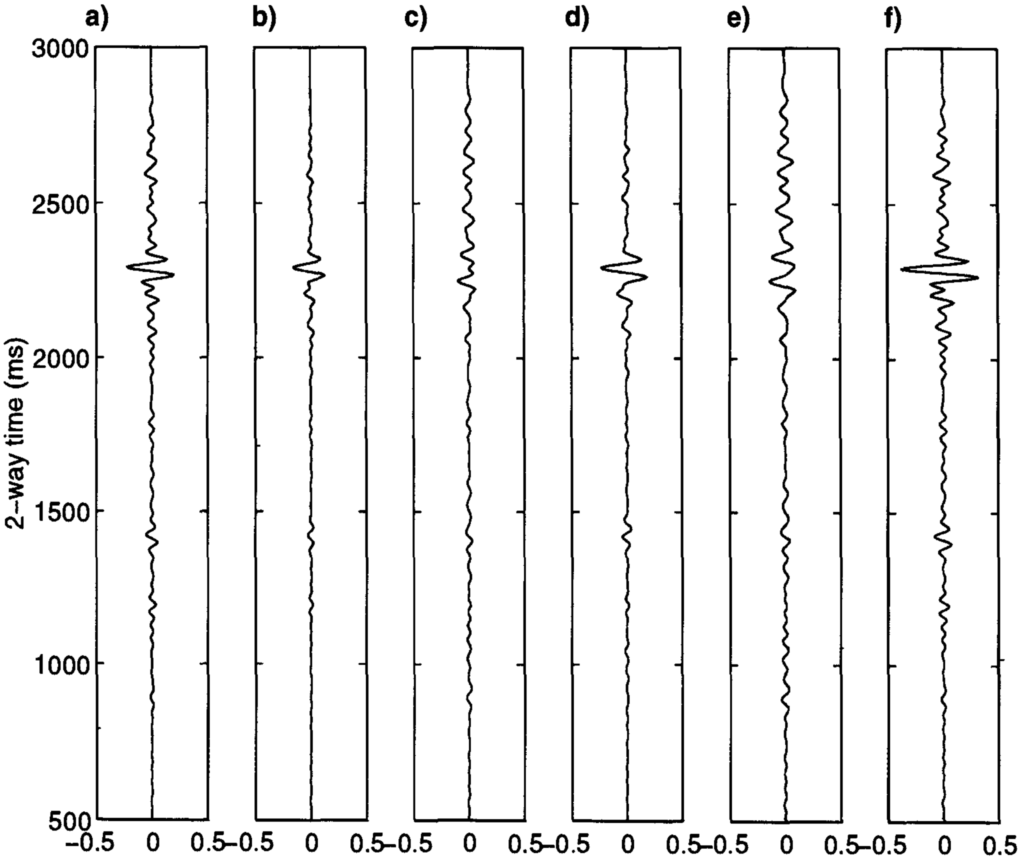

FIG. 14. Comparison of six estimated reflectivities from the linear inversion job in which the reflectivities and an anisotropic source are estimated (experiment 5). The reflectivity estimates shown above are the relative short-scale fluctuation in the (a) P-wave impedance, (b) P-wave velocity, (c) S-wave velocity, (d) ratio of P-wave velocity to S-wave velocity, (e) shear modulus, and (f) combination of Lamé constants $\lambda + 2\mu$.

Texas Geophysical Parallel Computation Project, the Schlumberger Foundation, IBM, and The Rice Inversion Project. TRIP Sponsors for 1995 are Advance Geophysical, Amerada Hess, Amoco Production Co., Conoco Inc., Cray Research Inc., Discovery Bay, Exxon Production Research Co., Interactive Network Technologies, and Mobil Research and Development Corp.

REFERENCES

Abramowitz, M., and Stegun, I., Eds., 1965, Handbook of mathematical functions, with formulas, graphs, and mathematical tables: Dover Publ. Inc.

Aki, K., and Richards, P., 1980, Quantitative seismology: Theory and methods: W. H. Freeman & Co.

Beylkin, G., 1985, Imaging of discontinuities in the inverse scattering problem by inversion of a causal generalized radon transform: J. Math. Phys., **26**, 99–108.

Brysk, H., and McCowan, D., 1986, A slant-stack procedure for point-source data: Geophysics, **51**, 1370–1388.

Bube, K., Lailly, P., Sacks, P., Santosa, F., and Symes, W., 1988, Simultaneous determination of source wavelet and velocity profile using impulsive point-source data from a layered fluid: Geophys. J., **95**, 449–462.

Buhl, P., Stoffa, P., and Bryan, G., 1974, The application of homomorphic deconvolution to shallow-water marine seismology—Part II: real data: Geophysics, **39**, 417–426.

Canadas, G., and Kolb, P., 1986, Least-squares inversion of prestack data: simultaneous identification of density and velocity of stratified media: 56th Ann. Internat. Mtg., Soc. Expl. Geophys., Expanded Abstracts, 604–607.

Castagna, J., Batzle, M., and Eastwood, R., 1985, Relationships between compressional-wave and shear-wave velocities in clastic silicate rocks: Geophysics, **50**, 571–581.

Castagna, J., and Smith, S., 1994, Comparison of avo indicators: A modeling study: Geophysics, **59**, 1849–1855.

Christensen, R., 1982, Theory of viscoelasticity: an introduction: Academic Press Inc.

Eisenstat, S., Elman, H., and Schultz, M., 1983, Variational iterative methods for nonsymmetric systems of linear equations: SIAM J. Number. Anal., **20**, 345–357.

Fletcher, R., 1980, Practical methods of optimization, i:unconstrained optimization: John Wiley & Sons, Inc.

Gauthier, O., Tarantola, A., and Virieux, J., 1986, Two-dimensional nonlinear inversion of seismic waveforms: Geophysics, **51**, 1387–1403.

Gockenbach, M., Symes, W., and Tapia, R., 1995, The dual regularization approach to seismic velocity inversion: Inverse Problems, **11**, No. 3, 501–531.

Igel, H., 1993, Seismic modeling and inversion: Ph.D. thesis, Institut de Physique du Globe de Paris.

Kern, M., and Symes, W., 1994, Inversion of reflection seismograms by differential semblance analysis: algorithm structure and synthetic examples: Geophys. Prosp., **42**, 565–614.

Lewis, R., 1989, Source-velocity identification for a layered model of reflection seismology: Ph.D. thesis, Department of Mathematical Sciences, Rice University.

Martinez, R., and McMechan, G., 1991a, τ-P seismic data for viscoelastic media—Part 1: Modeling: Geophys. Prosp., **39**, 141–156.

——— 1991b, $\tau - p$ seismic data for viscoelastic media—Part 2: Linearized inversion: Geophys. Prosp., **39**, 157–181.

Minkoff, S., and Symes, W., 1995, Estimating the energy source and reflectivity by seismic inversion: Inverse Problems, **11**, 383–395.

Pan, G., Young, C., and Castagna, J., 1993, Net pay delineation of gas sand using integrated target-oriented prestack elastic waveform inversion: 63th Ann. Internat. Mtg., Soc. Expl. Geophys., Expanded Abstracts, 431–434.

Robinson, E., 1967, Predictive decomposition of time series with application to seismic exploration: Geophysics, **32**, 418–484.

Sacks, P., 1990, A velocity inversion problem involving an unknown source: SIAM J. Appl. Math., **50**, No. 3, 931–941.

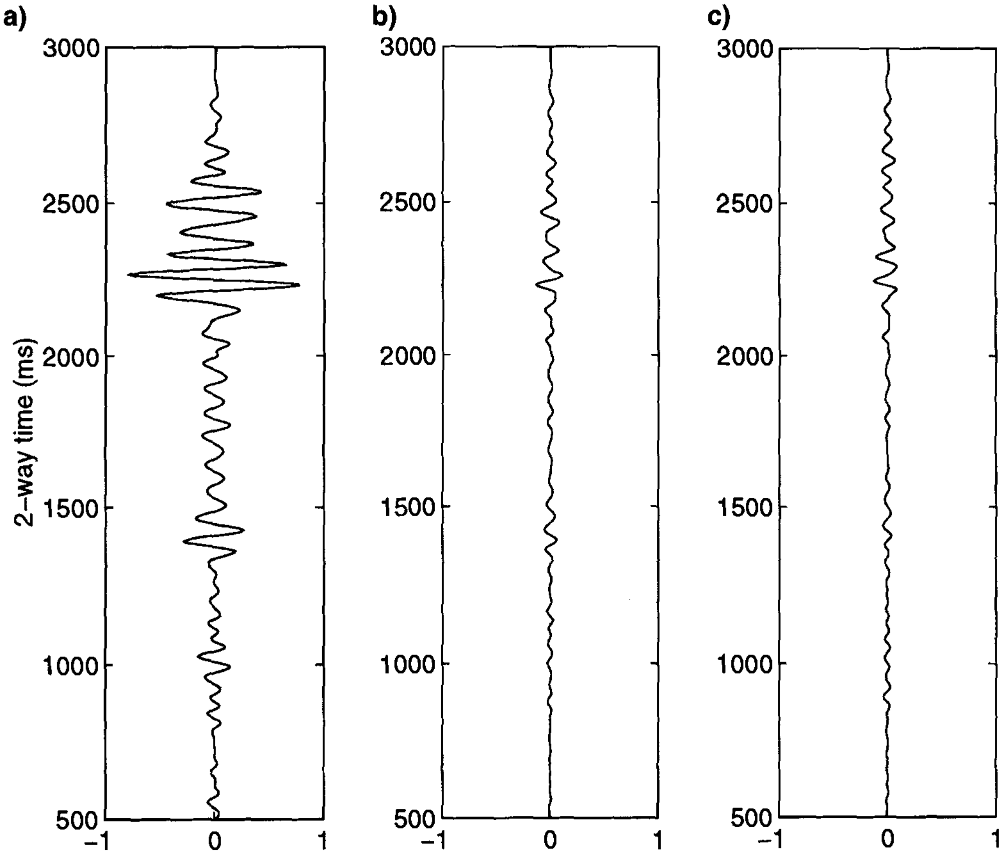

FIG. 15. Comparison of the relative short-scale fluctuation in the shear modulus which we determined by performing an inversion with (a) the air-gun model source (experiment 3), (b) an isotropic inversion-estimated source (experiment 4), and (c) an anisotropic inversion-estimated source (experiment 5). The shear moduli have all been shifted and scaled along with the other parameters gotten via inversion so the P-wave impedance inversion result matches the log.

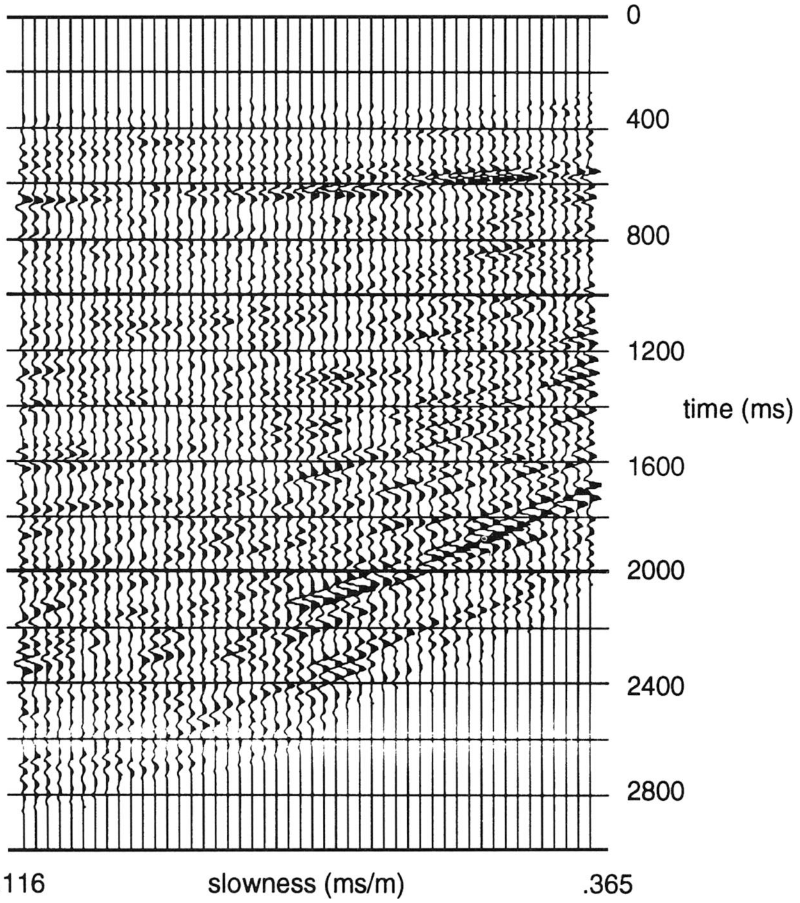

FIG. 16. The difference between the filtered, *ungained* CMP6 data and the data predicted by an *elastic* model. Misfit plotted on the scale of the data. Figure 3 (dark solid line) shows the background velocity. We estimated the reflectivities and energy source using inversion (experiment 7).

Sacks, P., and Symes, W., 1987, Recovery of the elastic parameters of a layered half-space: Geophys. J. Roy. Astr. Soc., **88**, 593–620.

Scales, J., Smith, M., and Fischer, T., 1991, Global optimization methods for highly nonlinear inverse problems, *in* Cohen, G., Halpern, L., and Joly, P., Eds., Mathematical and Numerical Aspects of Wave Propagation Phenomena:: Soc. for Indust. and Appl. Math., 434–444.

Sen, M., and Stoffa, P., 1991a, Nonlinear multiparameter optimization using genetic algorithms: Inversion of plane wave seismograms: Geophysics, **56**, 1794–1810.

——— 1991b, Nonlinear one-dimensional seismic waveform inversion using simulated annealing: Geophysics, **56**, 1624–1636.

Song, H., 1994, On a transmission inverse problem: Ph.D. thesis, Dept. of Computation and Applied Math: Rice University.

Stoffa, P., Buhl, P., and Bryan, G., 1974, The application of homomorphic deconvolution to shallow-water marine seismology—Part I: models: Geophysics, **39**, 401–416.

Symes, W., and Carazzone, J., 1991, Velocity inversion by differential semblance optimization: Geophysics, **56**, 654–663.

——— 1992, Velocity inversion by coherency optimization, *in* Bednar, J., Ed., Geophysical Inversion:: Soc. for Indust. and Appl. Math., 59–89.

Treitel, S., Gutowski, P., and Wagner, D., 1982, Plane-wave decomposition of seismograms: Geophysics, **47**, 1375–1401.

Ulrych, T., 1971, Application of homomorphic deconvolution to seismology: Geophysics, **36**, 650–660.

Wood, W., 1993, Linearized least-squares inversion of field seismic data for an elastic 1-D earth: 63th Ann. Internat. Mtg., Soc. Expl. Geophys., Expanded Abstracts, 661–664.